International Journal of Heat and Mass Transfer 52 (2009) 3055–3063

Contents lists available at ScienceDirect

International Journal of Heat and Mass Transfer

journal homepage: www.elsevier.com/locate/ijhmt

# A study of the Sherwood–Rayleigh relation for water undergoing natural convection-driven evaporation

S.M. Bower, J.R. Saylor *

*Clemson University, Department of Mechanical Engineering, Clemson, SC 29634-0921, USA*

ARTICLE INFO

*Article history:*
Received 14 August 2008
Received in revised form 14 January 2009
Accepted 14 January 2009
Available online 21 March 2009

*Keywords:*
Evaporation
Natural convection
Free surface

ABSTRACT

An experimental study is presented of evaporative free-surface natural convection. A power law relationship is developed between the Sherwood number for evaporation ($Sh$) and the Rayleigh number for air-side natural convection ($Ra$). Evaporation of water was investigated in sixteen different tanks having four depths and four widths. Evaporation rates and the relevant temperatures and relative humidity were measured, from which the air-side Sherwood and Rayleigh numbers were obtained. The resulting power law is $Sh \sim Ra^{0.321}$. This power law is compared to those obtained by other researchers. A brief discussion of the possible effect of water-side natural convection on evaporation is also presented.



## 1. Introduction

Demands on freshwater supplies for industrial, agricultural and human needs make important the ability to predict evaporation rates from inland bodies of water such as reservoirs and lakes [1–4], ponds [5], cooling impoundments [6], swimming pools [7], and livestock ponds [8]. The focus of the present study is evaporation from a water surface where natural convection is the dominant transport mechanism. Such a situation is not uncommon when wind speeds are small.

Field studies of evaporation from inland water bodies comprise a large body of literature. These studies, almost exclusively, seek to predict evaporation rates using equations of the form:

$$\dot{m}'' = f(\bar{u})(e_s - e_\infty) \tag{1}$$

where $\dot{m}''$ is the evaporation rate, $f(\bar{u})$ is a function of the mean wind speed $\bar{u}$, $e_s$ is the saturation vapor pressure at the water surface temperature, and $e_\infty$ is the vapor pressure in the air [9]. Other environmental parameters, such as lake size, are often included in Eq. (1). Field studies typically seek to fit data to a wind speed function $f(\bar{u})$ having the form:

$$f(\bar{u}) = a + b\bar{u} \tag{2}$$

originally suggested by Penman [10], where $a$ and $b$ are fitting constants, obtained from the field data. Some examples of field studies which yield equations of the form presented in Eq. (1) are Kohler and Parmele [1] who give:

$$\dot{m}'' = \rho(0.181 + 0.00236\bar{u})(e_s - e_\infty) \tag{3}$$

where $\rho$ is the liquid water density[1] and Taga et al. [11], who found:

$$\dot{m}'' = (0.088403 + 0.001296\bar{u})(e_s - \gamma e_\infty)/h_{fg} \tag{4}$$

where $\gamma$ is the relative humidity, and $h_{fg}$ is the latent heat of vaporization for water. Space limitations preclude a detailed survey of the literature, and good surveys can be found in the work of Sartori [12], Sweers [13], and Warnaka and Pochop [2].

A drawback of parameterizing the evaporation rate using Eqs. (1) and (2) is that not all of the known processes that affect evaporation are included. For example, $a$ and $b$ are known to vary with climate, season, solar conditions, geographical location, lake size, etc. [12,13]. Hence the results of field studies like those cited above tend to lose their utility when the equations are applied to other lakes or different conditions. Although this approach is necessary in the interim to provide some level of predictive capability, a long-term goal should be to obtain an understanding of each of the physical processes that affect lake evaporation.

One such process is natural convection, which is the motivation for the present study. According to the form of the wind speed function in Eq. (2) when $\bar{u} = 0$, $f(\bar{u}) = a$ which, from Eq. (1) gives a linear relationship between the evaporation rate and the driving vapor pressure difference, *viz.* the mass transfer coefficient ($h_m$, defined below) is a constant. Hence, equations of this form cannot predict the effect of natural convection on evaporation.

For small inland water bodies, conditions of low wind speed, where natural convection dominates, are not uncommon. For

* Corresponding author. Tel.: +1 864 656 5621; fax: +1 864 656 4435.
*E-mail address:* jrsaylor@ces.clemson.edu (J.R. Saylor).

[1] Note that the units used in Eq. (3) are not SI, as is the case for all other equations in this paper.

0017-9310/$ - see front matter © 2009 Elsevier Ltd. All rights reserved.
doi:10.1016/j.ijheatmasstransfer.2009.01.034

**Nomenclature**

| | |
|---|---|
| $A$ | surface area ($m^2$) |
| $B$ | *Sh*—*Ra* power law prefactor |
| $C$ | *Nu*—*Ra* power law prefactor |
| $D$ | tank depth (m) |
| $\mathscr{D}$ | diffusion coefficient ($m^2/s$) |
| $e$ | water vapor pressure ($N/m^2$) |
| $g$ | gravitational acceleration ($m/s^2$) |
| $h$ | heat transfer coefficient ($W/m^2$ K) |
| $h_{fg}$ | latent heat of vaporization for water (kJ/kg) |
| $h_m$ | mass transfer coefficient (m/s) |
| $k$ | thermal conductivity (W/m K) |
| $L^*$ | characteristic length, $A/P$ (m) |
| $m$ | *Nu*—*Ra* power law exponent |
| $\dot{m}''$ | mass flux ($kg/m^2$ s) |
| $n$ | *Sh*—*Ra* power law exponent |
| $Nu$ | Nusselt number |
| $P$ | tank perimeter (m) |
| $Ra$ | Rayleigh number |
| $Sc$ | Schmidt number |
| $Sh$ | Sherwood number |
| $T$ | temperature (°C) |
| $u$ | wind speed (m/s) |
| $W$ | tank width (m) |

*Greek symbols*

| | |
|---|---|
| $\alpha$ | thermal diffusivity of liquid water ($m^2/s$) |
| $\beta$ | coefficient of volumetric expansion ($K^{-1}$) |
| $\gamma$ | relative humidity (%) |
| $\nu$ | kinematic viscosity ($m^2/s$) |
| $\rho$ | density ($kg/m^3$) |

*Subscripts*

| | |
|---|---|
| $a$ | air |
| $b$ | bulk water, or beaker |
| $\infty$ | ambient |
| $s$ | surface |
| $sat$ | saturation |
| $t$ | tank |
| $tot$ | total |
| $wv$ | water vapor |

example a 10 year study of wind speed over Lake Sparkling in northern Wisconsin showed that the average wind speed during the summer was 2.3 m/s [14]. For the southeastern portion of the U.S. the average wind speed is less than 3 m/s for half of the year and the same is true for most of the continental U.S. for the months of June, July and August [15]. Similar results have been reported in the United Kingdom [16]. A long duration measurement campaign over a pond at the DOE Savannah River Site (SRS) in Aiken, South Carolina shows a peak in the wind speed probability density function at $u < 2$ m/s [17].

While the need to predict evaporation rates under natural convection dominated conditions exists, the body of literature on this subject is relatively limited. This literature consists of laboratory studies wherein a dimensionless mass transfer coefficient for evaporation, the Sherwood number, is related to natural convection through the Rayleigh number using a power law of the form:

$$Sh \sim Ra^n \tag{5}$$

where $Sh$ is the Sherwood number, defined as:

$$Sh = \frac{h_m W}{\mathscr{D}} \tag{6}$$

and $W$ is the characteristic length (a horizontal dimension in this study), and $\mathscr{D}$ is the diffusion coefficient for water vapor in air. The mass transfer coefficient for evaporation, $h_m$ is:

$$h_m = \dot{m}''/\Delta\rho_{wv} \tag{7}$$

where:

$$\Delta\rho_{wv} = \rho_{wv,s} - \gamma\rho_{wv,\infty} \tag{8}$$

Here, $\rho_{wv,s}$ and $\rho_{wv,\infty}$ are the saturated vapor densities evaluated at the water surface temperature $T_s$ and ambient air temperature $T_\infty$, respectively, and $\gamma$ is the relative humidity in the ambient. The Rayleigh number, $Ra$, is defined as:

$$Ra = \frac{g\Delta\rho W^3}{\bar{\rho}\nu\alpha} \tag{9}$$

where, $g$ is the gravitational acceleration, $\nu$ and $\alpha$ are the kinematic viscosity and thermal diffusivity or air, respectively, and:

$$\Delta\rho = \rho_\infty - \rho_s \tag{10}$$

where $\rho_s$ and $\rho_\infty$ are the air/vapor mixture densities at the water surface and ambient, respectively, and $\bar{\rho}$ is the average of $\rho_s$ and $\rho_\infty$.

A total of five studies were found which relate $Sh$ to $Ra$ for natural convection conditions. Sparrow et al. [18] studied evaporation using a series of water-filled pans in a 70 $m^3$ cork-lined room. Pans having diameters ranging from 8.89 cm to 30.68 cm were studied. For the case where the water level was flush with the tank rim (the condition closest to that used in the present study, where the meniscus was slightly above the tank rim), Sparrow et al. [18] found:

$$Sh = 0.764 Sc^{1/3} Ra^{0.205} \tag{11}$$

where $Sc$ is the Schmidt number, defined as:

$$Sc = \frac{\nu}{\mathscr{D}}. \tag{12}$$

We note that in the actual work of Sparrow et al. [18], the Schmidt number dependence is ignored. That is, the term $Sc^{1/3}$ does not appear and is implicitly included in the prefactor. Here, and in the presentation of subsequent literature, we have rewritten the *Sh*—*Ra* relationships developed by each author in the form:

$$Sh = BSc^{1/3} Ra^n \tag{13}$$

to enable comparison of the prefactors from different studies where different working fluids were used.

A unique aspect of the work of Sparrow et al. [18] was that for all of their experimental runs, the water temperature was less than the air temperature, resulting in a buoyancy-driven downflow. That is, the air/vapor mixture moved from the ambient towards the water. In the experiments presented herein, the water temperature was greater than the ambient, resulting in an upflow.

Sharpley and Boelter [19] and Boelter et al. [20], both using the same experimental facility, investigated evaporation of heated water from a pan into a 'quiet air apparatus.' Specifically, a one foot diameter pan was placed in a $5 \times 5 \times 7$ foot chamber, with vents connecting the chamber to the laboratory air. The resulting *Sh*—*Ra* relationship is:

$$Sh = 4.687 Sc^{1/3} Ra^{0.121} \tag{14}$$

for Boelter et al. [20] and

$$Sh = 1.254 Sc^{1/3} Ra^{0.213} \quad (15)$$

for Sharpley and Boelter [19]. Due to slight differences in the definitions of the relevant dimensionless groups from those used here, Eqs. (14) and (15) were obtained by reprocessing the actual data presented in Boelter et al. [20] and Sharpley and Boelter [19] to conform to the definitions of *Sh* and *Ra* used here. It should also be noted that the Sharpley and Boelter [19] data set included very small as well as negative values of *Ra*; at times the water surface temperature was less than the ambient. These data were excluded when developing Eq. (15).

Goldstein et al. [21] investigated the sublimation of naphthalene from planforms of square, rectangular and circular shape into a quiescent air environment having a volume of 110 $m^3$. Although sublimation differs from evaporation in that the interfacial hydrodynamic boundary condition is no-slip, there is nevertheless a similarity in that this study still investigates mass transfer due solely to natural convection. The *Sh*—*Ra* relation that they obtained was:

$$Sh = 0.435 Sc^{1/3} Ra^{0.250} \quad (16)$$

In order to collapse their (*Sh*, *Ra*) data obtained from different geometry planforms, Goldstein et al. [21] employed the length scale,

$$L^* = A/P \quad (17)$$

in their definition of *Sh* and *Ra*, where *A* is the planform surface area and *P* is the perimeter.

Lloyd and Moran [22] studied mass transfer in the presence of natural convection using an electrochemical method. This electrochemical method created a density difference above a horizontal copper plate in a solution $H_2SO_4$ and $CuSO_4$, and $Cu^{2+}$ ions were the quantity transported. As in the work of Goldstein et al. [21], Lloyd and Moran [22] used $L^*$ as their characteristic length. The resulting *Sh*—*Ra* relation was:

$$Sh = 0.038 Sc^{1/3} Ra^{0.255} \quad (18)$$

for the laminar regime where $2.2 \times 10^4 < Ra < 8.0 \times 10^6$, and

$$Sh = 0.013 Sc^{1/3} Ra^{0.327} \quad (19)$$

for the turbulent regime where $8.0 \times 10^6 < Ra < 1.6 \times 10^9$. As for the case of Goldstein et al. [21], this study differs from actual evaporative transport in the existence of a no-slip boundary condition at the mass transfer interface.

The five studies cited above are compiled in tabular form in Table 1, with each *Sh*—*Ra* relationship rewritten in the form of Eq. (13).

The above survey of the literature reveals that a large amount of work has been done which attempts to parameterize the evaporation rate on lakes and other inland water bodies to wind speed, as well as other factors. However, we have been able to identify only five studies which quantify mass transfer under purely natural convection conditions. One of the motivations of the present study is to expand on this relatively small body of research. Additionally, of the five studies cited above, only three actually pertained to the evaporative transport of water. Of these three citations, the work of Sparrow et al. [18] pertains only to conditions where the water is colder than the air, resulting in a density gradient that drives a downflow in the air, the opposite of what would typically occur on heated water bodies. Finally, in the work of Boelter et al. [20] and Sharpley and Boelter [19], the flow of air was restricted by the close proximity of the evaporation pan to the wall of the quieting chamber, as well as by vertical baffles which were introduced to reduce air motion. Those authors noted that these restrictions significantly changed the evaporation rate. It seems then, that a study of the *Sh*—*Ra* relationship has not been conducted for evaporation from a water body where the air flow is relatively unrestricted, a situation more like that which occurs on a pond undergoing pure natural convection. The absence of such a study is the second motivation for the work presented here.

**Table 1**
Comparison of *Sh*—*Ra* power law prefactors and exponents from the present work and earlier studies. Note that for the results presented in lines 6–8, the length scale used is $L^*$ (Eq. (17)). To facilitate comparison with these three studies, the present work has been reformulated using this length scale in line 5.

| Parameterization | $Sh = BSc^{1/3}Ra^n$ | | | |
|---|---|---|---|---|
| | *B* | *n* | *Sc* | *Ra* range |
| 1. Present study | 0.230 | 0.321 | 0.60 | $9.6 \times 10^5 < Ra < 5.7 \times 10^8$ |
| 2. Sharpley and Boelter [19] | 1.057 | 0.213 | 0.60 | $10^6 < Ra < 4.5 \times 10^7$ |
| 3. Boelter et al. [20] | 0.645 | 0.241 | 0.60 | $9.3 \times 10^6 < Ra < 4.6 \times 10^8$ |
| 4. Sparrow et al. [18] | 0.764 | 0.205 | 0.60 | $-6 \times 10^5 < Ra < -2 \times 10^4$ |
| 5. Present study (using $L^*$) | 0.196 | 0.322 | 0.60 | $2 \times 10^4 < Ra_{L^*} < 9 \times 10^6$ |
| 6. Goldstein et al. [21] | 0.435 | 0.250 | 2.5 | $2 \times 10^2 < Ra_{L^*} < 5 \times 10^3$ |
| 7. Lloyd and Moran [22] | 0.013 | 0.327 | 2200 | $8 \times 10^6 < Ra_{L^*} < 1.6 \times 10^9$ |
| 8. Lloyd and Moran [22] | 0.038 | 0.255 | 2200 | $2 \times 10^4 < Ra_{L^*} < 8 \times 10^6$ |

## 2. Experimental method

Experiments were conducted using a set of insulated glass tanks, all of which were different in either depth or width. The tanks were filled with warm tap water and allowed to cool down in a quiescent laboratory environment for 1–2 h while data were collected. The measurements included: the bulk water temperature, $T_b$, the surface temperature of the water, $T_s$, the room air temperature, $T_\infty$, the room relative humidity, $\gamma$, and the mass loss due to evaporation, $\dot{m}''$. From these data, *Sh* and *Ra* were calculated and power law fits were subsequently generated. A schematic of the experimental apparatus is shown in Fig. 1.

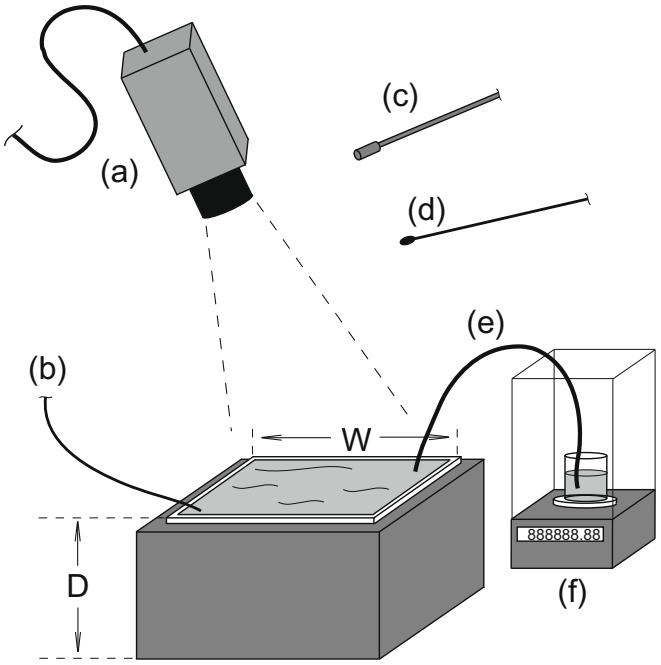


**Fig. 1.** Diagram of the experimental facility showing an insulated tank of width, *W*, and depth, *D*, (a) infrared camera for surface temperature measurements, (b) water bulk temperature sensor, (c) relative humidity probe, (d) air temperature probe, (e) water siphon tube, and (f) electronic balance for evaporation measurement.

The bulk water temperature was measured with a Fluke 5611T thermistor (±0.01 °C) and the air temperature was measured with a General Electric CSP60BA103M-H/2-90 thermistor (±0.01 °C). These data were logged with a Hart Scientific 1529 Chub-E4 Thermometer Readout (±0.002 °C accuracy and 0.0001 °C resolution). The surface temperature was measured by processing digital imagery taken with an Inframetrics Thermacam SC1000 infrared camera (±0.07 K) with a platinum silicide 255 × 239 focal plane array sensor, sensitive to infrared light in the 3.4–5 μm wavelength band. Prior to the experiments, the camera was calibrated with an Infrared Systems Development Corporation model IR-140/301 Blackbody Source (emissivity of 0.96 ± 0.02%) and Controller System (±0.2 *K* accuracy and 0.1 K resolution). For measuring the room relative humidity, $\gamma$, a Digi-Sense Thermohygrometer data logger and probe were used (0.1% relative humidity resolution and accuracy of ±0.2% of reading). Mass was measured using a Scientech Zeta Series ZSA210 electronic balance (±0.15 mg accuracy, ±0.2 mg linearity and 0.1 mg resolution).

The water tanks were made of 9.5 mm thick glass and silicone RTV (type 110) adhesive and were constructed with depths of 5.1, 10.2, 15.2, and 35.5 cm and widths of 15.2, 30.5, 45.7, and 60.9 cm. All tank footprints were square. All combinations of these depths and widths were explored, resulting in a total of 16 tanks. Two layers of 1.9 cm thick Perma "R" expanded polystyrene panel foam were used to insulate the sides and bottom of each tank to minimize heat loss through the tank walls.

Each tank was filled with tap water at approximately 43 °C such that the interface was pinned at the tank rim and the meniscus was slightly above the rim. The $T_b$ thermocouple was located at tank mid-depth. It is assumed that the tank fluid is well-mixed by natural convection, and hence that $T_b$ is representative of the bulk fluid temperature. The $T_\infty$ thermocouple and the relative humidity probe were placed sufficiently far from the tank setup to not disturb air flow at the water surface. The distance from the IR camera lens to the water surface was 46 cm, and the camera was mounted approximately 25° from vertical.

The evaporative mass loss was measured by running a flexible siphon tube (91 cm in length, 4.5 mm in diameter) from the tank to a small beaker of water located on the weighing pan inside the balance enclosure. Thus, as water from the tank evaporated, water flowed through the siphon tube from the beaker into the tank, resulting in a decrease in the mass measured by the balance. Measures were taken to increase the relative humidity of the environment within the balance enclosure in order to prevent significant evaporation of water from the beaker. Nevertheless, finite evaporation occurred and a separate set of experiments were performed to correct for this, in which the siphon tube was disconnected and the beaker evaporation was recorded. This beaker evaporation rate was subtracted from the measured evaporation rate for each experimental run. Upon filling the tank with water, the system was allowed to sit for 1 h prior to acquiring data.

The mass flux from the tank, $\dot{m}''$, was obtained from:

$$\dot{m}'' = \frac{(dm/dt)_b}{A_b} = \frac{(dm/dt)_t}{A_t} \tag{20}$$

where $A_b$ and $A_t$ are the surface areas of the air/water interface for the beaker and tank, respectively, and $\frac{dm}{dt}$ is the time rate of change of the mass of water. The mass data from the beaker were fit with an exponential curve. The derivative $\frac{dm}{dt}$ was obtained from the analytical derivative of this curve fit; derivatives of other quantities required in this work were also obtained from analytical derivatives of the relevant curve fits. The surface temperature data, $T_s$, were fit with exponential curves as well. A linear least-squares regression was used to fit the $\gamma$ and $T_\infty$ data since these varied very little during the course of an experimental run. The temperature sensitivity of the fluid properties was accounted for when calculating $h_m$, *Sh*, and *Ra* using the tabular data from Chapman [23], except for the diffusion coefficient, $\mathscr{D}$, which was obtained from the equation:

$$\mathscr{D}_T = \mathscr{D}_{298}\left(\frac{T}{298\ \mathrm{K}}\right)^{3/2} \tag{21}$$

which is valid assuming the air/vapor mixture is an ideal gas, and that there is no variation in pressure [24].

The method for obtaining the densities used in Eqs. (8) and (10) follows the procedure presented in Sparrow et al. [18]. The density of water vapor in the air is obtained from:

$$\rho_{wv,\infty} = \gamma \rho_{sat}(T_\infty) \tag{22}$$

where $\rho_{sat}(T_\infty)$ is obtained from the steam tables [25]. The air/vapor mixture density is obtained by:

$$\rho_\infty = \rho_{a,\infty} + \rho_{wv,\infty} \tag{23}$$

and $\rho_{a,\infty}$ is obtained from the ideal gas law with temperature set to $T_\infty$ and pressure set to:

$$p_{a,\infty} = p_{tot} - p_{wv,\infty} \tag{24}$$

and $p_{tot}$ set to one atmosphere. The densities at the surface are obtained using the same method as shown in Eqs. (22)–(24). That is, the mixture density at the surface is:

$$\rho_s = \rho_{a,s} + \rho_{wv,s} \tag{25}$$

where $\rho_{wv,s} = \rho_{sat}(T_s)$. The air density at the surface, $\rho_{a,s}$, is obtained from the ideal gas law in a manner similar to Eq. (24).

We note that, contrary to the work of Sparrow et al. [18], $\Delta\rho$ in Eq. (10) is defined to be positive when the air/vapor mixture at the surface is less dense than the surrounding air. Finally it should be noted that $\Delta\rho$ accounts for temperature effects and air/vapor density differences, and should not be confused with the $\Delta\rho_{wv}$ from Eq. (8) used in $h_m$ which describes only the difference in water vapor densities.

A physical description of the evaporative and convective behavior of the system under study is presented in Fig. 2. Heat loss at the water surface occurs primarily through evaporation and natural convection with the air. This surface water cools, becomes more dense and descends through the bulk layer towards the bottom. The displaced warmer fluid rises through the bulk towards the surface. On the air-side of the interface, a buoyant plume structure forms due to two factors: (i) $T_s$ is greater than $T_\infty$, and (ii) the relatively high concentration of water vapor at the surface makes the air/vapor mixture there less dense than the surrounding air. Hence, in a problem of this type, it is important to use $\Delta\rho$ in *Ra* from Eq. (9) instead of $\beta\Delta T$ as is often done when defining *Ra*.

## 3. Results

Time traces are presented in Fig. 3 for $T_b$, $T_\infty$, $T_s$, and $\gamma$ from a sample experiment. As noted in the previous section, $\gamma$ and $T_\infty$ exhibit little variation during the course of an experiment, and this is

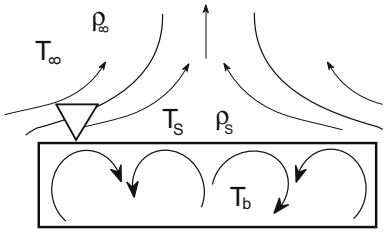


**Fig. 2.** Schematic of the transport processes at the air-side and water-side of the surface of a water tank.

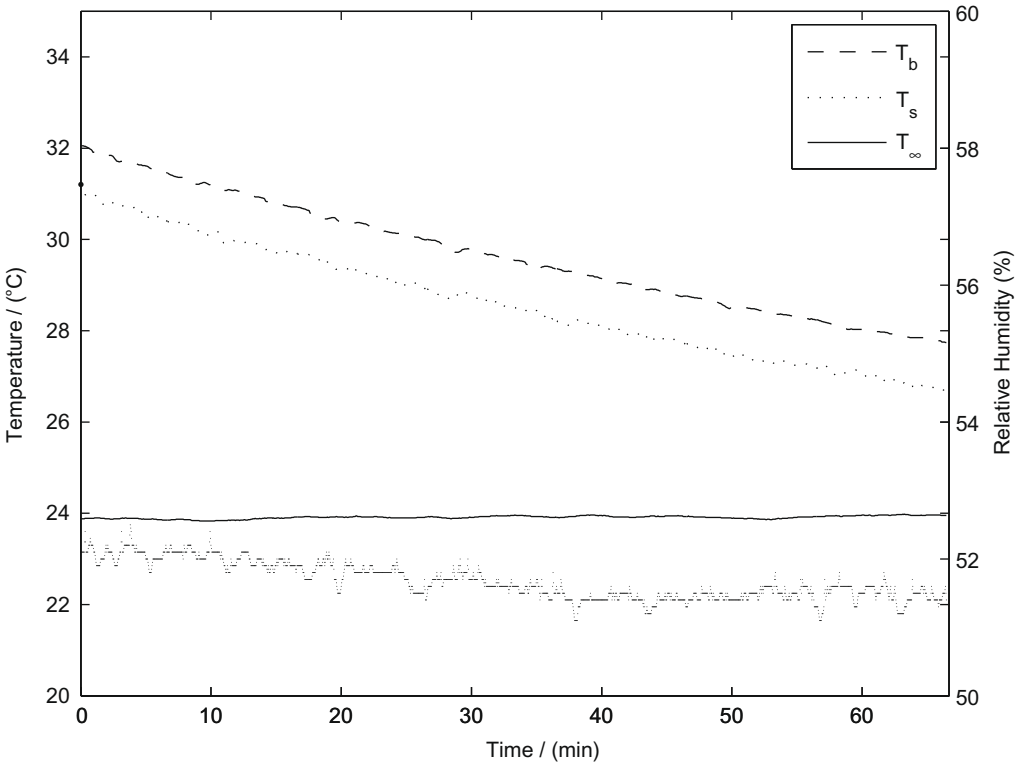


**Fig. 3.** Time trace of the bulk water, surface, and air temperatures and the relative humidity (lowest line in the plot) for a sample experimental run.

confirmed in Fig. 3. The mass data obtained for the beaker, also from a sample run, are shown in Fig. 4 along with the corresponding tank evaporation rate, calculated from the derivative of the exponential curve fit to the mass data.

A total of 63 experiments were conducted in this investigation, each with time traces similar to those shown in Figs. 3 and 4. The data were reduced to $h_m$ using Eq. (7) and are plotted against $\Delta\rho/\bar{\rho}$ (Eq. (10)) in Fig. 5 where each line represents a single experimental run. In Fig. 5, $h_m$ behaves as expected in that $h_m$ increases with $\Delta\rho/\bar{\rho}$. There are a few experimental runs where $h_m$ actually decreases with $\Delta\rho/\bar{\rho}$. While the reason for this behavior is unclear, the number of these anomalous runs is small and do not significantly affect the conclusions. It should be noted that this and subsequent figures show quantities that are obtained from curve fits to the raw data. Hence, individual data points are not presented.

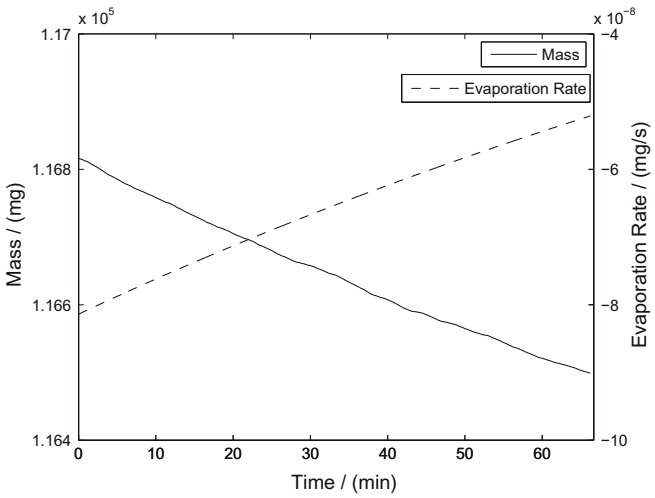


**Fig. 4.** Time series of the mass loss in the balance apparatus due to evaporation and the corresponding time derivative.

The product of *Sh* and *Ra* is plotted against *Ra* in Fig. 6. In this figure, *ShRa* is plotted instead of *Ra* alone to reduce the effect of errors in the measurement of $\Delta T$. Such errors propagate into $\Delta\rho$ since $\Delta\rho = \Delta\rho(\Delta T, \gamma)$. Therefore, $\Delta T$ is intrinsically present in the numerator of *Ra* in Eq. (9) and in the denominator of *Sh* via $\Delta\rho_{wv}$ in $h_m$ from Eq. (7). Thus, by plotting *ShRa* versus *Ra*, the inclusion of errors in $\Delta T$ in both axes is avoided. The combined uncertainty of measurement and fitting errors results in an error in *Ra* of $\pm 2.04\%$ and an error in *ShRa* of $\pm 0.62\%$ (the uncertainty in *Sh* was $\pm 1.95\%$). The prefactors and exponents of the *Sh*—*Ra* power laws were obtained from a linear least-square fit to the logarithm of both *Ra* and *ShRa*. The resulting power law exponent, *n*, shown in Eq. (13) becomes $(n+1)$ when using the *ShRa*—*Ra* parameterization while the prefactor, *B*, remains the same. Henceforth, 1.0 has been subtracted from the exponent obtained in the *ShRa*—*Ra* power law relation to enable comparison to *Sh*—*Ra* power law relations in the literature. Finally, it is noted that the range in *Ra* in Fig. 6 was obtained in two ways, first by using tanks of different width, and secondly via the range in $\Delta T$ that existed during the course of each experimental run.

## 4. Discussion

The main results of this work are summarized in Fig. 6. This plot of *ShRa* versus *Ra* yields the following power law:

$$Sh = 0.230 Sc^{1/3} Ra^{0.321} \tag{26}$$

This result was obtained for a range of *Ra* spanning three decades. The uncertainty in the exponent is $\pm 0.0096$ and the uncertainty in the prefactor is $\pm 0.0383$. It is noted that *n* in Eq. (26) differs from $1/3$ by less than 4%. This result is of particular interest for two rea-

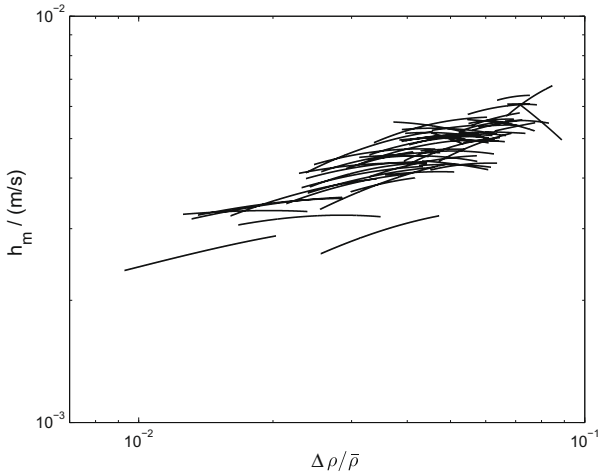


**Fig. 5.** Plot of $h_m$ versus $\Delta\rho/\bar{\rho}$ for all runs.

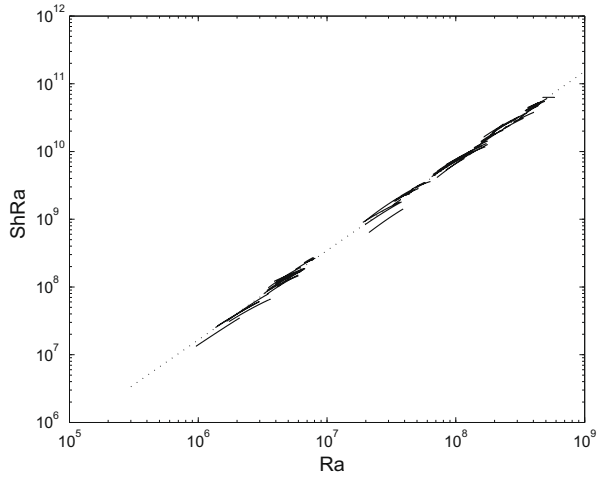


**Fig. 6.** The air-side *ShRa*—*Ra* power law represented by the dotted line, which gives $B = 0.230$ and $n = 0.321 + 1$. Data were acquired using tanks having widths of 15.2 cm, 30.5 cm, 45.7 cm, and 60.9 cm.

sons. First, a value close to 1/3 is often found for the exponent $m$ in turbulent natural convection heat transfer studies using a power law relation between the Nusselt and Rayleigh numbers:

$$Nu = CRa^m \tag{27}$$

where the Nusselt number is defined as:

$$Nu = hL/k \tag{28}$$

Here, $h$ is the heat transfer coefficient, $L$ is the characteristic length usually defined as the vertical distance between the heated/cooled plates in the traditional Rayleigh–Bénard setup, and $k$ is the thermal conductivity of the fluid. For example, Globe and Dropkin [26] found $m = 1/3$, Chu and Goldstein [27] show $m = 0.278$, and Niemela et al. [28] give $m = 0.309$ for a range of *Ra* spanning 11 orders of magnitude. Many other studies exist, and a good review is provided in Chavanne et al. [29] who show that with few exceptions $m \cong 0.3$. The similarity between $m$ and the value of $n$ attained here exists in spite of the fact that the present investigation concerns mass transfer in parallel with heat transfer, as opposed to pure heat transfer, and the boundary conditions are very different. For example, in Rayleigh–Bénard convection experiments, typically there is a solid plate bounding the top and the bottom of a fluid layer, making the problem one where the hydrodynamic boundary condition is of the no-slip kind. In the present experiment, the air resides above an air/water interface which is a free surface and therefore lacks the no-slip boundary condition. Moreover, there is (effectively) no upper boundary for the air, and the length scale used in this study is the width of the tank, a horizontal scale, while in the Rayleigh–Bénard case, the length scale is the vertical distance between the two solid plates. The fact that we attain such a similar value for the power law exponents $m$ and $n$ in spite of these differences suggests a certain robustness in the power law relationship between these two dimensionless heat and mass transfer coefficients (*viz.* the Nusselt and Sherwood numbers) and the Rayleigh number. Furthermore, this suggests that the characteristics of turbulence that control the transport are more important than the specific details of the boundary conditions or even the quantity being transported (mass versus heat).

The second reason the similarity of $n$ to 1/3 is significant concerns the characteristic length in the definition of *Ra* and *Sh*. Below, the *Sh*—*Ra* power law correlation from Eq. (13) is shown in expanded form using $n = 1/3$:

$$\frac{h_m W}{\mathscr{D}} = BSc^{1/3}\left(\frac{g(\rho_\infty - \rho_s)W^3}{\bar{\rho}\nu\alpha}\right)^{\frac{1}{3}} \tag{29}$$

which allows for the cancellation of the characteristic length, and reduces to:

$$h_m \sim \left(\frac{\rho_\infty - \rho_s}{\bar{\rho}}\right)^{1/3} \sim \left(\frac{\Delta\rho}{\bar{\rho}}\right)^{1/3} \tag{30}$$

showing that the characteristic length has no effect on $h_m$ when $n = 1/3$. The fact that the value of $n$ obtained here is very close to 1/3 indicates a corresponding lack of sensitivity of $h_m$ to length scale for evaporation driven by natural convection, at least under the conditions explored here.

Table 1 presents the exponents and prefactors for the *Sh*—*Ra* power law obtained from the present study and those studies cited in Section 1. The Schmidt number for the working fluid used in each study is also presented. In lines 1–4 of Table 1, the length scale used in the definition of *Ra* and *Sh* is the typical characteristic length, namely the width or diameter of the water tank or pan. In lines 5–8, the length scale $L^*$ (Eq. (17)) is used in computing *Ra* and *Sh*. This is because Goldstein et al. [21] and Lloyd and Moran [22] employed planforms of several different geometries necessitating the use of this length scale to collapse their data. To facilitate comparison with these two studies, the present data is also reformulated using $L^*$, and the resulting prefactor and exponent are presented in line 5. It is noted that the magnitude of the Rayleigh numbers attained when using $L^*$ as a length scale are significantly reduced. Finally we note that two entries are provided for the work of Lloyd and Moran [22], line 7 for their turbulent results and line 8 for the laminar results.

The exponent obtained in the present work is significantly larger than that obtained by the other studies presented in the first four lines of Table 1, 45% larger than the average of these three other studies. The effect of this difference in $n$ can be seen in Fig. 7 where the present data has been plotted along with that obtained from the studies cited in lines 2 and 3, graphically showing the difference in slope. In lines 5–8 of Table 1 our exponent is very close to the turbulent value of Lloyd and Moran [22] (which differs from the present value by less than 2%), and different from the remaining studies, both of which give exponents close to 1/4.

A possible explanation for the difference/similarity between $n$ from the present work and the cited literature concerns the range in *Ra* pursued in these studies, and in the effect of airflow restriction on evaporation. Referring to lines 2–4 of Table 1, $n$ increases monotonically with the maximum *Ra* explored in the study. The

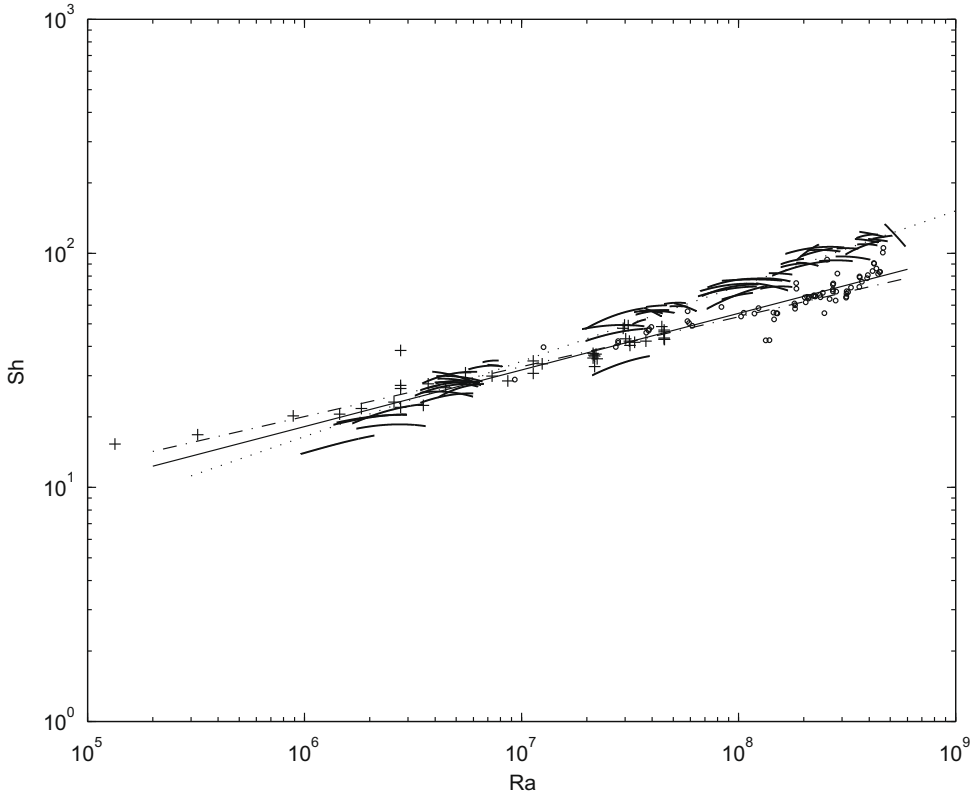


**Fig. 7.** Comparison of the present results (dotted power law line and solid data lines) with those of Sharpley and Boelter (dash-dot line and + data symbols) and Boelter et al. (solid line and circles) on *Sh* versus *Ra* coordinates.

present work has a maximum *Ra* larger than all three of those studies, and has the largest *n*. Of course, the maximum *Ra* of the present study is only slightly larger than that of Boelter et al. [20] ($5.7 \times 10^8$ compared to $4.6 \times 10^8$), yet the difference in *n* is large. Hence, additional explanation is needed. As noted in Section 1, the studies cited in lines 2–4 were all conducted in facilities where the flow of air to the water tank or pan was significantly restricted, at least compared to the present work where the water tank was placed in a laboratory without a housing or other structure to impede air flow. It is possible that this is the other factor that accounts for the larger *n* found here compared to the aforementioned authors. That is, our value of *n* is larger because the flow of air above the water is less restricted, enabling *Sh* to increase more readily with increasing *Ra*.

A similar argument can be made for the studies cited in lines 6–8 of Table 1. Here, the work of Goldstein et al. [21] results in $n = .250$ for values of $Ra_{L^*}$ much smaller than that attained in the present study, supporting the idea that *n* is small when the Rayleigh numbers are relatively small. The work of Lloyd and Moran [22] yield *n* very close to that attained herein when their values of $Ra_{L^*}$ are significantly larger than that of the present study. They also attain a value of *n* that is smaller than ours when their range in $Ra_{L^*}$ is comparable to ours. Again, a possible explanation is that, in Lloyd and Moran [22], the flow restrictions inherent in their apparatus result in a small exponent ($n = 0.255$) even when the $Ra_{L^*}$ range is essentially the same as the present work.

The above discussion tends to suggest that smaller values of *n* will be attained at lower *Ra*, at least below some limiting value of *Ra*. This confirms prior work which has shown that $n = 1/4$ for low *Ra*, but increases at larger *Ra* [20]. There is abundant research in the heat transfer literature to suggest that above a relatively low value of *Ra*, $m \cong 0.3$ with relatively small changes in *m* with increasing *Ra*, similar to what is seen here with evaporation [26–29].

Finally, we raise the somewhat subtle question of whether water-side natural convection can affect evaporation. To first order, any effect of water-side motion should be accounted for in the air-side definitions of *Ra* and *Sh*. For example, vigorous natural convection on the water side could easily change the surface temperature, and hence evaporation rate, however such a change in $T_s$ is accounted for in the variables $\rho_{wv,s}$ and $\rho_s$ used in Eqs. (8) and (10), which are in turn used in the present definitions of *Sh* and *Ra*. On the other hand, one might argue that for a given average $T_s$, two different tanks having different *water-side* Rayleigh numbers due to different depths will have different water-side turbulence intensities giving, for example, a different value for the root mean square of $T_s$. The question then is: will such an effect have an impact on *Sh*? The data acquired here can begin to address this question, since tank depth *D* was varied.

Fig. 8 presents *Sh* plotted against $Ra_D$, which is the water-side Rayleigh number defined as:

$$Ra_D = \frac{g\beta\Delta T D^3}{\nu\alpha} \tag{31}$$

where $\beta$ is the volume expansivity, *D* is the tank depth, $\Delta T = T_b - T_s$, and all fluid properties are for liquid water. The curve fits are coded according to tank width revealing, as expected, a strong vertical separation of the data according to width. The plot also shows, however, a small increase in *Sh* with $Ra_D$ for each tank width, tempting one to surmise that water-side natural convection plays a role in evaporative transport. These data are now replotted in Fig. 9(a) on $h_m$ versus $Ra_D$ coordinates, also showing a slight increase with depth. In Fig. 9(b), representative runs are plotted on $h_m$ versus $T_s$ coordinates. Careful observation of Fig. 9(a) and (b) shows that $h_m$ increases both with $T_s$ and with depth. That is, Fig. 9(b) shows that for each progressively deeper tank, $T_s$ becomes higher. This may in fact be due to an experimental artifact. Namely, due to the procedure of waiting 1 h prior to initiating data acquisition, the shallower

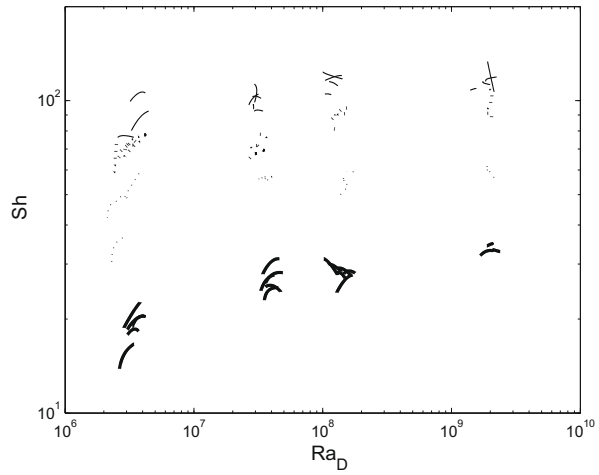


**Fig. 8.** Plot of *Sh* versus water-side Rayleigh number $Ra_D$. Line type is according to tank *width*: thick solid line – 15.2 cm; thin dotted line – 30.5 cm, thick dashed line – 45.7 cm; and thin solid line – 60.9 cm.

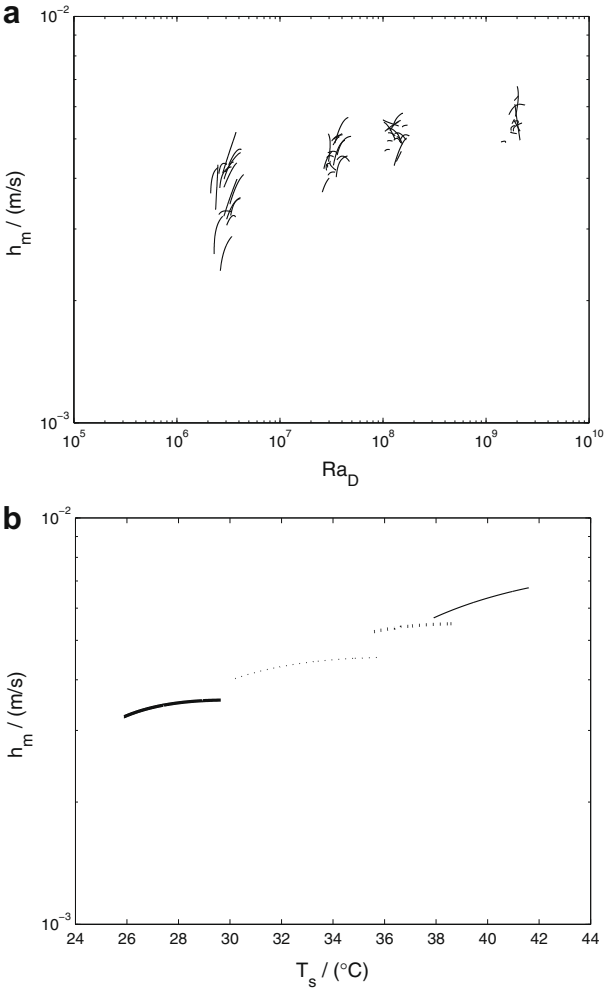


**Fig. 9.** (a) Plot of $h_m$ versus the water-side Rayleigh number, $Ra_D$. (b) Plot of $h_m$ versus $T_s$. In (a), the data are clumped according to tank *depth*, from left to right: $D = 5.1$ cm, 10.2 cm, 15.2 cm, and 35.5 cm. In (b) a single representative time trace is presented for each tank *depth* to reveal the apparent trend. Depth: thick solid line – 5.1 cm; thin dotted line – 10.2 cm; thick dashed line – 15.2 cm; and thin solid line – 35.5 cm.

tank runs started at a significantly lower initial $T_s$ than the deeper tanks. Hence Fig. 9(b) may be showing larger $h_m$ in deeper tanks simply because these tanks had larger values for $T_s$. Since the air temperatures were relatively constant, this larger $T_s$ corresponds to a larger air-side $\Delta T$ and a correspondingly larger air-side Rayleigh number. Thus what seems like an effect of depth may simply be that deeper tanks had larger air-side Rayleigh numbers, resulting in larger *Sh*.

To determine whether water depth can affect the evaporation rate, experiments conducted at constant tank width over a range of tank depths would be needed with the critical requirement that the range of air-side $\Delta T$ overlap for the different tank depths. Since $T_\infty$ is essentially a constant, this requirement is essentially that the range of $T_s$ be the same for each tank depth. As shown in Fig. 9(b), there is essentially no overlap in $T_s$ for all four tank depths evaluated in this work, preventing us from making a conclusive statement one way or the other regarding the effect of depth. Overall, this effect is not expected to be large, but may have some significance in environmental applications where very large depth variations exist.

## 5. Conclusion

Data were collected from a set of water tanks undergoing natural convection-driven evaporation. These data were reduced to a dimensionless mass transfer coefficient for evaporation, *Sh*, and related to the air-side Rayleigh number *Ra* via a power law. The resulting *Sh*—*Ra* power law exponent was $n = 0.321 \pm 0.0096$ and the prefactor was $B = 0.230 \pm 0.0383$. The value of the exponent is close to 1/3, a value similar to power law exponents obtained in many *Nu*—*Ra* studies of natural convection heat transfer. The similarity between these power law equations suggests that the characteristics of turbulence dictate transport phenomena in a way that transcends the relevant length scale, or even the quantity being transported. At the same time, comparison with prior laboratory studies of evaporation suggests restriction of air flow in the vicinity of the evaporating surface can significantly affect *n*. Finally, comparison with prior work confirms that a value of *n* close to 1/3 is not achieved until *Ra* is sufficiently large.

## Acknowledgments

This research was supported by the National Science Foundation through Grant No. 0500155, and the Department of Energy through the Savannah River National Laboratory. Support from these agencies is gratefully acknowledged.

## References

[1] M.A. Kohler, L.H. Parmele, Generalized estimates of free-water evaporation, Water Resour. Res. 3 (1967) 997–1005.
[2] K. Warnaka, L. Pochop, Analyses of equations for free water evaporation estimates, Water Resour. Res. 24 (1988) 979–984.
[3] E.K. Webb, A pan-lake evaporation relationship, J. Hydrol. 4 (1966) 1–11.
[4] F.I. Morton, Operational estimates of lake evaporation, J. Hydrol. 66 (1983) 77–100.
[5] C.E. Boyd, Pond evaporation, Trans. Am. Fish. Soc. 114 (1985) 299–303.
[6] E.E. Adams, D.J. Cosler, K.R. Helfrich, Evaporation from heated water bodies: predicting combined forced plus free convection, Water Resour. Res. 26 (1990) 425–435.
[7] C.C. Smith, G. Löf, R. Jones, Measurement and analysis of evaporation from an inactive outdoor swimming pool, Sol. Energy 53 (1994) 3–7.
[8] J.L. Duesterhaus, J.M. Ham, C.E. Owensby, J.T. Murphy, Water balance of a stock-watering pond in the Flint Hills of Kansas, Rangeland Ecol. Manage. 61 (2008) 329–338.
[9] W. Brutsaert, Evaporation into the Atmosphere: Theory, History, and Applications, D. Reidel Publishing Company, Dordrecht, Holland, 1982.
[10] H.L. Penman, Natural evaporation from open water, bare soil and grass, Proc. R. Soc. Lond. A 193 (1948) 120–145.

[11] M. Taga, T. Matsumoto, T. Ochi, Studies on membrane viscosity stabilized solar pond, Sol. Energy 45 (1990) 315–324.
[12] E. Sartori, A critical review on equations employed for the calculation of the evaporation rate from free water surfaces, Sol. Energy 68 (2000) 78–89.
[13] H.E. Sweers, A nomogram to estimate the heat-exchange coefficient at the air–water interface as a function of wind speed and temperature: a critical survey of some literature, J. Hydrol. 30 (1976) 375–401.
[14] J.D. Lenters, T.K. Kratz, Effects of climate variability on lake evaporation: results from a long-term energy budget study of Sparkling Lake, northern Wisconsin (USA), J. Hydrol. 308 (2005) 168–195.
[15] K. Klink, Climatological mean interannual variance of United States surface wind speed, direction and velocity, Int. J. Climatol. 19 (1999) 471–488.
[16] D.M. Deaves, I.G. Lines, The nature and frequency of low wind speed conditions, J. Wind Eng. 73 (1998) 1–29.
[17] Allen Weber, SRNL, personal communication.
[18] E.M. Sparrow, G.K. Kratz, M.J. Schuerger, Evaporation of water from a horizontal surface by natural convection, J. Heat Transfer 105 (1983) 469–475.
[19] B.F. Sharpley, L.M.K. Boelter, Evaporation of water into quiet air from a one-foot diameter surface, Ind. Eng. Chem. 30 (1938) 1125–1131.
[20] L.M.K. Boelter, H.S. Gordon, B.F. Sharpley, Free evaporation into air of water from a free horizontal quiet surface, Ind. Eng. Chem. 38 (1946) 596–600.
[21] R.J. Goldstein, E.M. Sparrow, D.C. Jones, Natural convection mass transfer adjacent to horizontal plates, Int. J. Heat Mass Transfer 16 (1973) 1025–1035.
[22] J.R. Lloyd, W.R. Moran, Natural convection adjacent to horizontal surface of various planforms, J. Heat Transfer 96 (1974) 443–447.
[23] A. Chapman, Fundamentals of Heat Transfer, MacMillan Publishing Company, New York, 1987.
[24] R.B. Bird, W.E. Stewart, E.N. Lightfoot, Transport Phenomena, John Wiley & Sons, New York, 1960.
[25] F.P. Incropera, D.P. DeWitt, Fundamentals of Heat and Mass Transfer, fourth ed., John Wiley & Sons, 1996.
[26] S. Globe, D. Dropkin, Natural-convection heat transfer in liquids confined by two horizontal plates and heated from below, J. Heat Transfer 81 (1959) 24–28.
[27] T.Y. Chu, R.J. Goldstein, Turbulent convection in a horizontal layer of water, J. Fluid Mech. 60 (1973) 141–159.
[28] J.J. Niemela, L. Skrbek, K.R. Sreenivasan, R.J. Donnelly, Turbulent convection at very high Rayleigh numbers, Nature 404 (2000) 837–840.
[29] X. Chavanne, F. Chillà, B. Chabaud, B. Castaing, B. Hébral, Turbulent Rayleigh–Bénard convection in gaseous and liquid He, Phys. Fluids 13 (2001) 1300–1320.